Supporting Information:

Environment-Assisted Quantum Transport through Single-Molecule Junctions

Jakub K. Sowa Jan A. Mol G. Andrew D. Briggs Erik M. Gauger

October 18, 2017

Contents

S1 Theoretical Methods

S1.1 The Electronic Hamiltonian

Let us begin by motivating the choice of the electronic Hamiltonian H_M [Eq. (2)] described in the main body of the manuscript. Our system consists of two aromatic sites (coupled to the source or the drain electrode) connected by a saturated link. Let us consider two localised

molecular orbitals, $|L\rangle$ and $|R\rangle$ (one at each of the sites), which are coupled to each other with the strength J. As mentioned in the manuscript, they themselves are not eigenstates of the molecular Hamiltonian which are instead given by:

$$|\Psi_+\rangle = \cos\theta\,|L\rangle + \sin\theta\,|R\rangle\ ; \tag{S1}$$

$$|\Psi_-\rangle = \sin\theta\,|L\rangle - \cos\theta\,|R\rangle\ . \tag{S2}$$

Here, the mixing angle θ is given by $\tan 2\theta = -2J/\Delta\varepsilon$, where $\Delta\varepsilon = \varepsilon_R - \varepsilon_L$. Let us also remark that for $J < 0$ (as used in this work) the bonding orbital $|\Psi_+\rangle$ is lower in energy.

Alternatively, one may start these considerations from a pair of closely spaced molecular orbitals, $|\Psi_+\rangle$ and $|\Psi_-\rangle$, of a bonding and antibonding character (in the case of molecular system studied by Perrin *et al.* in Ref. [1] both the HOMO/HOMO-1 and LUMO/LUMO+1 pairs satisfy this condition [2]). Then, the $|L\rangle$ and $|R\rangle$ states can be obtained directly from equations (S1) and (S2).

As further justification of our approach, we note that the transport characteristics (calculated in the absence of environmental interactions) of our adopted two-site model yield very similar results to those obtained from DFT+NEGF methods, for a number of molecular systems [1, 3].

We will now proceed under the assumption that our system is governed by the Hamiltonian described in the main body of the manuscript, and outline the various theoretical methods used in our study.

S1.2 Pure dephasing & Redfield approaches

We begin by considering the well-known second order quantum master equation [4]:

$$\frac{\mathrm{d}\rho(t)}{\mathrm{d}t} = -\mathrm{i}[H_S, \rho(t)] - \int_0^t \mathrm{d}\tau\ \mathrm{Tr}_E\left[H_I, \left[\tilde{H}_I(-\tau), \rho(t)\rho_E\right]\right]\ , \tag{S3}$$

where H_S and H_I are referred to as the system and the interaction Hamiltonians respectively, ρ_E denotes the density matrix of the thermalised environment (comprising two fermionic reservoirs

and two phonon baths), and $\tilde{}$ denotes the interaction picture of H_S. In the case of our system $H_S \equiv H_M$, and $H_I \equiv H_C + H_V$. Since (within the Born approximation) terms linear in H_V vanish, the quantum master equation is given by:

$$\frac{\mathrm{d}\rho(t)}{\mathrm{d}t} = -\mathrm{i}[H_M, \rho(t)] + \mathcal{L}_{leads}\rho(t) + \mathcal{L}_{ph}\rho(t) \ . \tag{S4}$$

The superoperators in Eq. (S4) are:

$$\mathcal{L}_{leads}\rho(t) = -\int_0^\infty \mathrm{d}\tau \ \mathrm{Tr}_E \ \Big[H_V, [\tilde{H}_V(-\tau), \rho(t)\rho_E]\Big] \ ; \tag{S5}$$

$$\mathcal{L}_{ph}\rho(t) = -\int_0^\infty \mathrm{d}\tau \ \mathrm{Tr}_E \ \Big[H_C, [\tilde{H}_C(-\tau), \rho(t)\rho_E]\Big] \ . \tag{S6}$$

In the above, anticipating that our interest will lie in the steady-state dynamics we have extended the integration limit to infinity. Let us note here that in charge transport through nanoscopic systems, non-Markovian effects generally have a small effect on the values of steady-state (average) electric current (our primary observable) but can have a more significant influence on higher current cumulants such as the zero-frequency noise or skewness [5, 6].

The superoperator $\mathcal{L}_{leads}\rho(t)$ is evaluated by expanding the commutators in Eq. (S5) yielding:

$$\begin{aligned}\mathcal{L}_{leads}\rho(t) = -\sum_{j,k_j}\int_0^\infty \mathrm{d}\tau \Big[& h_{k_j}(\tau)\left(a_j\tilde{a}_j^\dagger(-\tau)\rho(t) - \tilde{a}_j^\dagger(-\tau)\rho(t)a_j\right) \\ & + \bar{h}_{k_j}(-\tau)\left(a_j^\dagger\tilde{a}_j(-\tau)\rho(t) - \tilde{a}_j(-\tau)\rho(t)a_j^\dagger\right) \\ & + h_{k_j}(-\tau)\left(\rho(t)\tilde{a}_j(-\tau)a_j^\dagger - a_j^\dagger\rho(t)\tilde{a}_j(-\tau)\right) \\ & + \bar{h}_{k_j}(\tau)\left(\rho(t)\tilde{a}_j^\dagger(-\tau)a_j - a_j\rho(t)\tilde{a}_j^\dagger(-\tau)\right)\Big] \ .\end{aligned} \tag{S7}$$

Here, $h_{k_j}(\tau) \equiv |V_{k_j}|^2 \, f_j(\epsilon_{k_j}) \, e^{\mathrm{i}\epsilon_{k_j}\tau}$, $\bar{h}_{k_j}(\tau) \equiv |V_{k_j}|^2 \, [1 - f_j(\epsilon_{k_j})] \, e^{\mathrm{i}\epsilon_{k_j}\tau}$ with the Fermi distribution given by: $f_j(\epsilon_{k_j}) = \mathrm{Tr}_{res}(R_0 c_{k_j}^\dagger c_{k_j}) = 1/(e^{(\epsilon_{k_j}-\mu_j)/kT}+1)$, and μ_j is the chemical potential of the lead $j = L, R$.

Fourier decomposition $\left[\tilde{A}(\tau) = \sum_\xi e^{-\mathrm{i}\xi\tau}A(\xi)\right]$ of the creation and annihilation operators in Eq. (S7), reveals that they oscillate only at the frequencies corresponding to molecular orbital

energies,

$$\tilde{a}_L(\tau) = \left(\frac{\Delta\varepsilon+\eta}{2\eta}a_L - \frac{J}{\eta}a_R\right)e^{-\mathrm{i}\varepsilon_+\tau} + \left(\frac{-\Delta\varepsilon+\eta}{2\eta}a_L + \frac{J}{\eta}a_R\right)e^{-\mathrm{i}\varepsilon_-\tau} \ , \tag{S8}$$

$$\tilde{a}_R(\tau) = \left(-\frac{J}{\eta}a_L - \frac{\Delta\varepsilon-\eta}{2\eta}a_R\right)e^{-\mathrm{i}\varepsilon_+\tau} + \left(\frac{J}{\eta}a_L + \frac{\Delta\varepsilon+\eta}{2\eta}a_R\right)e^{-\mathrm{i}\varepsilon_-\tau} \ , \tag{S9}$$

where $\Delta\varepsilon = \varepsilon_R - \varepsilon_L$, $\eta = \sqrt{\Delta\varepsilon^2 + 4J^2}$. Analogous expressions can be found for $\tilde{a}_L^\dagger(\tau)$ and $\tilde{a}_R^\dagger(\tau)$, and we can also confirm that for each of these operators $\sum_\xi A(\xi) = A$.

The integral over τ in Eq. (S7) can be evaluated using

$$\int_0^\infty \mathrm{d}\tau e^{\pm\mathrm{i}\Omega\tau} = \pi\delta(\Omega) \pm \mathrm{i}\frac{\mathcal{P}}{\Omega} \ ,$$

where $\mathcal{P}$ denotes Cauchy principal value. Finally, the sum over the energy levels k_i in the leads can be replaced by an integral and evaluated within the wide band approximation (WBA), $V_{k_i} = V_i$ for all k_i. We will henceforth ignore the imaginary parts of (S7); their effect is a slight renormalisation of terms that already present in the system Hamiltonian and whilst small, they do not, in general, converge within WBA mathematically.

S1.2.1 Pure Dephasing

The pure dephasing approach involves replacing the superoperator $\mathcal{L}_{ph}$ in Eq. (S4) with

$$\mathcal{L}_{deph}\rho(t) = \frac{1}{2}\Gamma_D \sum_{j=L,R} \left(2n_j\rho(t)n_j - n_j\rho(t) - \rho(t)n_j\right) \ , \tag{S10}$$

where $n_j = a_j^\dagger a_j$. This Lindbladian superoperator describes an exponential decay of coherences [off-diagonal elements of $\rho(t)$] in the site basis, at the rate Γ_D. The phenomenological superoperator given in Eq. (S10) can be motivated by the form of the electron-phonon coupling Hamiltonian H_C which acts as the number operator on the electronic subspace. It is important to bear in mind here that pure dephasing displays infinite-temperature characteristics. The limitations of pure dephasing will be discussed in Section S4.

S1.2.2 Redfield approach

By contrast, the Redfield approach involves evaluating the phononic dissipator [Eq. (S6)] which takes the form:

$$\begin{aligned}\mathcal{L}_{ph}\rho(t) = -\sum_{j=L,R}\int_0^\infty \mathrm{d}\tau \left[C_j^R(\tau)\left(n_j\tilde{n}_j(-\tau)\rho(t) - \tilde{n}_j(-\tau)\rho(t)n_j\right)\right. \\ \left. + C_j^R(-\tau)\left(\rho(t)\tilde{n}_j(-\tau)n_j - n_j\rho(t)\tilde{n}_j(-\tau)\right)\right] ,\end{aligned} \tag{S11}$$

where we have once again utilised the Markovian approximation. Let us stress that the Eq. (S11) takes this form due to our assumption that each of the sites is coupled to an independent phonon bath. The correlation functions in Eq. (S11) are given by [7]:

$$C_j^R(\tau) = \int_0^\infty \mathrm{d}\omega\, \mathcal{J}_j(\omega)\left[\cos(\omega\tau)\coth(\beta\omega/2) - \mathrm{i}\sin(\omega\tau)\right] , \tag{S12}$$

where $\mathcal{J}_j(\omega)$ is a spectral density defined in the main body of the manuscript. Let us note here that we shall not ignore the phonon-induced renormalisations of the Hamiltonian (which will be given by the imaginary parts of the response functions in Eq. (S11)).

S1.3 The Polaron Method

S1.3.1 Polaron transformation

The first step in the derivation of the Quantum Master Equation (QME) in the polaron frame is the polaron (Lang-Firsov) transformation [8] which eliminates the electron-phonon coupling Hamiltonian (H_C),

$$\bar{H} = e^G H e^{-G} \tag{S13}$$

where

$$G = \sum_{j=L,R}\sum_{q_j} g_{q_j} a_j^\dagger a_j (b_{q_j}^\dagger - b_{q_j}) . \tag{S14}$$

This leads to the transformed Hamiltonian:

$$\bar{H} = \bar{H}_\mathrm{M} + H_\mathrm{B} + \bar{H}_\mathrm{V} + H_\mathrm{R} , \tag{S15}$$

where

$$\bar{H}_{\mathrm{M}} = \sum_{j=L,R} \bar{\varepsilon}_j a_j^\dagger a_j + J\left(B_L^\dagger B_R\, a_L^\dagger a_R + \mathrm{H.c.}\right) , \tag{S16}$$

and

$$\bar{H}_{\mathrm{V}} = \sum_{k_L,k_R} V_{k_L} B_L c_{k_L}^\dagger a_L + V_{k_R} B_R c_{k_R}^\dagger a_R + \mathrm{H.c.} \, . \tag{S17}$$

Here, $\bar{\varepsilon}_j$ denotes the renormalised site energy $\bar{\varepsilon}_j = \varepsilon_j - \sum_q g_q^2/\omega_q$ (for consistency with the other approaches this renormalisation will be ignored – it changes the position of the levels with respect to the Fermi energy and has only a trivial effect on the system's dynamics), and B_j are the displacement operators:

$$B_j = \exp\left[-\sum_{q_j} \frac{g_{q_j}}{\omega_{q_j}} (b_{q_j}^\dagger - b_{q_j})\right] . \tag{S18}$$

S1.3.2 Quantum Master Equation

In this section we derive a QME describing the dynamics of the considered model system in the polaron frame. We start by redefining the Hamiltonian in terms of the system ($\bar{H}_S$), the environment ($H_E = H_R + H_B$) and the interaction Hamiltonian ($\bar{H}_I$). The system Hamiltonian is given by:

$$\bar{H}_S = \sum_{j=L,R} \varepsilon_j a_j^\dagger a_j + J\langle B_{LR}\rangle \left(a_L^\dagger a_R + \mathrm{H.c.}\right) \, . \tag{S19}$$

It accounts for the site energies, as well as the coupling between the sites. The latter is renormalised by $\langle B_{LR}\rangle = \langle B_L\rangle\langle B_R\rangle$, where $\langle ...\rangle$ denotes an average with respect to the thermal equilibrium and

$$\langle B_j\rangle = \langle B_j^\dagger\rangle = \exp\left(-\frac{1}{2}\int_0^\infty \mathrm{d}\omega \frac{\mathcal{J}_j(\omega)}{\omega^2} \coth(\beta\omega/2)\right) \, , \tag{S20}$$

where $\beta = 1/k_{\mathrm{B}}T$, with Boltzmann constant k_{B}.

The interaction Hamiltonian is now defined as $\bar{H}_I = \bar{H}_V + \bar{H}_P$, where:

$$\bar{H}_P = J\left[\left(B_L^\dagger B_R - \langle B_{LR}\rangle\right) a_L^\dagger a_R + \mathrm{H.c.}\right] \, . \tag{S21}$$

Analogously to Eq. (S4), the QME can be written in the form:

$$\frac{\mathrm{d}\bar{\rho}(t)}{\mathrm{d}t} = -\mathrm{i}[\bar{H}_S, \bar{\rho}(t)] - \int_0^\infty \mathrm{d}\tau \ \mathrm{Tr}_E \ \left[\bar{H}_V, [\tilde{H}_V(-\tau), \bar{\rho}(t)\bar{\rho}_E]\right] - \int_0^\infty \mathrm{d}\tau \ \mathrm{Tr}_E \ \left[\bar{H}_P, [\tilde{H}_P(-\tau), \bar{\rho}(t)\bar{\rho}_E]\right] \ , \quad \text{(S22)}$$

or simply, $\dfrac{\mathrm{d}\bar{\rho}(t)}{\mathrm{d}t} = -\mathrm{i}[\bar{H}_S, \bar{\rho}(t)] + \mathcal{L}_{\text{leads}}\bar{\rho}(t) + \mathcal{L}_{\text{pol}}\bar{\rho}(t)$.

S1.3.3 Molecule-lead terms

Let us first evaluate the $\mathcal{L}_{\text{leads}}\bar{\rho}$ term given by:

$$\mathcal{L}_{\text{leads}}\bar{\rho}(t) = -\int_0^\infty \mathrm{d}\tau \ \mathrm{Tr}_E \ \left[\bar{H}_V, [\tilde{H}_V(-\tau), \bar{\rho}(t)\bar{\rho}_E]\right] \ . \quad \text{(S23)}$$

Expanding the commutator and tracing out the environmental degrees of freedom leads to:

$$\begin{aligned}\mathcal{L}_{leads}\bar{\rho}(t) = -\sum_{j,k_j}\int_0^\infty \mathrm{d}\tau \Big[& h_{k_j}(\tau)\langle B_j B_j^\dagger(-\tau)\rangle \left(a_j\tilde{a}_j^\dagger(-\tau)\bar{\rho}(t) - \tilde{a}_j^\dagger(-\tau)\bar{\rho}(t)a_j\right) \\ & + \bar{h}_{k_j}(-\tau)\langle B_j^\dagger B_j(-\tau)\rangle \left(a_j^\dagger\tilde{a}_j(-\tau)\bar{\rho}(t) - \tilde{a}_j(-\tau)\bar{\rho}(t)a_j^\dagger\right) \\ & + h_{k_j}(-\tau)\langle B_j(-\tau)B_j^\dagger\rangle \left(\bar{\rho}(t)\tilde{a}_j(-\tau)a_j^\dagger - a_j^\dagger\bar{\rho}(t)\tilde{a}_j(-\tau)\right) \\ & + \bar{h}_{k_j}(\tau)\langle B_j^\dagger(-\tau)B_j\rangle \left(\bar{\rho}(t)\tilde{a}_j^\dagger(-\tau)a_j - a_j\bar{\rho}(t)\tilde{a}_j^\dagger(-\tau)\right)\Big] \ .\end{aligned} \quad \text{(S24)}$$

The phononic correlation functions $C_j^P(\tau) \equiv \langle B_j(\tau)B_j^\dagger\rangle = \langle B_j^\dagger(\tau)B_j\rangle$ can be evaluated as follows:

$$C_j^P(\tau) = \langle B_j\rangle^2 \exp\left[\int_0^\infty \mathrm{d}\omega \ \frac{\mathcal{J}_j}{\omega^2}\left(\cos\omega\tau \coth\left(\frac{\beta\omega}{2}\right) - \mathrm{i}\sin\omega\tau\right)\right] \ . \quad \text{(S25)}$$

Once again, we will ignore the imaginary parts of Eq. (S25).

S1.3.4 Intra-molecular terms

Similar approximations will be made in evaluating the next term in Eq. (S22):

$$\begin{aligned}\mathcal{L}_{pol}\bar{\rho}(t) = &- |J|^2 \int_0^\infty \mathrm{d}\tau \\ &\Big\{ C_-^P(\tau)\left(s\tilde{s}(-\tau)\rho(t) - \tilde{s}(-\tau)\rho(t)s\right) + C_+^P(\tau)\left(s\tilde{s}^\dagger(-\tau)\rho(t) - \tilde{s}^\dagger(-\tau)\rho(t)s\right) \\ &+C_+^P(\tau)\left(s^\dagger\tilde{s}(-\tau)\rho(t) - \tilde{s}(-\tau)\rho(t)s^\dagger\right) + C_-^P(\tau)\left(s^\dagger\tilde{s}^\dagger(-\tau)\rho(t) - \tilde{s}^\dagger(-\tau)\rho(t)s^\dagger\right) \\ &+C_-^P(-\tau)\left(\rho(t)\tilde{s}(-\tau)s - s\rho(t)\tilde{s}(-\tau)\right) + C_+^P(-\tau)\left(\rho(t)\tilde{s}^\dagger(-\tau)s - s\rho(t)\tilde{s}^\dagger(-\tau)\right) \\ &+C_+^P(-\tau)\left(\rho(t)\tilde{s}(-\tau)s^\dagger - s^\dagger\rho(t)\tilde{s}(-\tau)\right) + C_-^P(-\tau)\left(\rho(t)\tilde{s}^\dagger(-\tau)s^\dagger - s^\dagger\rho(t)\tilde{s}^\dagger(-\tau)\right) \Big\} \,. \end{aligned} \tag{S26}$$

Here, $s \equiv a_L^\dagger a_R$, and the correlation functions are given by:

$$C_+^P(t) = \prod_{j=L,R}\langle B_j\rangle^2 \exp\left[\int_0^\infty \mathrm{d}\omega\, \frac{\mathcal{J}_j}{\omega^2}\left(\cos\omega\tau\coth\left(\frac{\beta\omega}{2}\right) - \mathrm{i}\sin\omega\tau\right)\right] - \langle B_L\rangle^2\langle B_R\rangle^2 \,, \tag{S27}$$

$$C_-^P(t) = \prod_{j=L,R}\langle B_j\rangle^2 \exp\left[-\int_0^\infty \mathrm{d}\omega\, \frac{\mathcal{J}_j}{\omega^2}\left(\cos\omega\tau\coth\left(\frac{\beta\omega}{2}\right) - \mathrm{i}\sin\omega\tau\right)\right] - \langle B_L\rangle^2\langle B_R\rangle^2 \,. \tag{S28}$$

Finally, let us notice that in the limit of high temperature and for a slowly fluctuating environment, the treatment used here can be reduced to the well-known Marcus theory. This is demonstrated on an example of a two-site (Donor–Acceptor) system in Section S5.

S1.4 The choice of basis

In this work we focus on the sequential tunnelling regime of transport. It is assumed that due to the strong Coulomb interactions only one additional (transport) electron can be found on the molecular wire at any given time. This assumption is typically well justified for molecular systems at moderate bias voltage, as verified by a number of experimental studies. Hence, the tight-binding basis comprises three electronic states corresponding to the additional charge density occupying each of the sites and the vacuum state (molecule in the neutral charge state). Transport beyond the sequential tunnelling case will be a focus of our future work.

S1.5 Observables

Here, we are interested in the steady-state solution of the relevant quantum master equation:

$$\frac{\mathrm{d}\rho}{\mathrm{d}t} = 0 \ , \tag{S29}$$

(and equivalently in the polaron transformed frame) which yields the stationary density matrix ρ_{stat} ($\bar{\rho}_{stat}$). The primary observable of interest, the steady-state value of current through the wire, is most easily found by considering the rates of electron hopping between either of the terminal sites and the leads. As demonstrated in Section S1.5.1, the value of the current at $j = L, R$ interface is given by the expectation value of the appropriate current operator:

$$I_j = \mathrm{Tr}(\mathcal{I}_j \bar{\rho}_{stat}) \ , \tag{S30}$$

where

$$\mathcal{I}_j\rho \ = \ \frac{\gamma_j}{2} \ \sum_k f_j(\xi_k) \left[a_j^\dagger(\xi_k)\rho a_j + a_j^\dagger \rho a_j(\xi_k)\right] \ - \ (1 - f_j(\xi_k)) \left[a_j(\xi_k)\rho a_j^\dagger + a_j \rho a_j^\dagger(\xi_k)\right] \quad , \tag{S31}$$

and equivalently in the polaron frame. Here, $\gamma_j = 2\pi|V_j|^2\varrho_j$ and ξ_k are the eigenvalues of the molecular Hamiltonian H_M. Let us note that, due to the current conservation, the steady-state currents at the two leads must be equal and opposite $I_L = -I_R$.

The average populations of the sites are given simply by the diagonal elements of ρ_{stat} or $\bar{\rho}_{stat}$ (which are invariant under the polaron transformation).

Lastly, we may want to consider the zero-frequency current noise $S(0)$. As shown by Flindt *et al.* [9]:

$$S(0)/2e^2 = \mathrm{Tr}\left[\left(\mathcal{I}_j^+ + \mathcal{I}_j^-\right)\rho_{\mathrm{stat}}\right] - 2\ \mathrm{Tr}\left[\left(\mathcal{I}_j^+ - \mathcal{I}_j^-\right)\mathcal{R}\left(\mathcal{I}_j^+ - \mathcal{I}_j^-\right)\rho_{\mathrm{stat}}\right] \ , \tag{S32}$$

where $\mathcal{I}_j^\pm$ are the superoperators describing electron hopping on/off the interface with j-lead. $\mathcal{R} = (1 - \mathcal{P})\mathcal{L}^{-1}(1 - \mathcal{P})$ is the Moore-Penrose pseudoinverse of $\mathcal{L}$ where $\mathcal{P}$ is the projection operator formed as an outer product of identity and ρ_{stat} vectors. The derivation of Eq. (S32) can be found in Refs. [9–11]

S1.5.1 Full counting statistics

The result shown in Eq. (S30) can be justified using the methods of full counting statistics (FCS) [9]. Consider a quantum master equation of the general form:

$$\frac{\mathrm{d}\rho(t)}{\mathrm{d}t} = \mathcal{L}\rho(t) \ , \tag{S33}$$

and let us introduce the n-resolved density matrix (where n is the number of electrons transferred between the molecule and one of the leads at time t). The n-resolved quantum master equation is then given by:

$$\frac{\mathrm{d}\rho^{(n)}(t)}{\mathrm{d}t} = \left(\mathcal{L} - \mathcal{I}_R^+ - \mathcal{I}_R^-\right)\rho^{(n)}(t) + \mathcal{I}_R^+\rho^{(n-1)}(t) + \mathcal{I}_R^-\rho^{(n+1)}(t) \ . \tag{S34}$$

Here, $\mathcal{I}_R^+$ ($\mathcal{I}_R^-$) is a superoperator that describes tunnelling out of (into) the molecular system at the interface with the right electrode. At any time t, $\sum_n \rho^{(n)}(t) = \rho(t)$.

Next, let us define the cumulant generating function:

$$e^{S(\chi,t)} = \sum_n P_n(t) e^{\chi n} = \mathrm{Tr}\left[\sum_n \rho^{(n)}(t)\ e^{\chi n}\right] \ , \tag{S35}$$

where $P_n(t)$ is the probability of n electrons being collected (in the right lead) during time t. Cumulants of the charge distribution can be obtained by considering derivatives of S with respect to the counting field χ,

$$\langle\langle n^{(m)}\rangle\rangle(t) = \left.\frac{\partial^m S(\chi,t)}{\partial\chi^m}\right|_{\chi=0} \ . \tag{S36}$$

The average (steady-state) electric current is then given by:

$$I = \frac{\mathrm{d}\langle\langle n\rangle\rangle(t)}{\mathrm{d}t} = \frac{\mathrm{d}}{\mathrm{d}t}\left.\frac{\partial S(\chi,t)}{\partial\chi}\right|_{\chi=0} \quad \text{at } t\to\infty \ . \tag{S37}$$

In order to evaluate this expression, let us consider the time dependence of $\rho_\chi(t) = \sum_n \rho^{(n)}(t)\ e^{\chi n}$.

From Eq. (S34), it is given by:

$$\dot{\rho}_\chi(t) = \left(\mathcal{L} - (1-e^{\chi})\mathcal{I}_R^+ - (1-e^{-\chi})\mathcal{I}_R^-\right)\rho_\chi(t) = \mathcal{L}_\chi \rho_\chi(t) \ , \tag{S38}$$

with a solution $\rho_\chi(t) = \exp(\mathcal{L}_\chi t)\ \rho_\chi(0)$, and $e^{S(\chi,t)} = \mathrm{Tr}\left[\rho_\chi\right]$. This yields:

$$I = \mathrm{Tr}\left[\left.\frac{\partial \mathcal{L}_\chi}{\partial \chi}\right|_{\chi=0} \rho_{stat}\right] = \ \mathrm{Tr}\left[\mathcal{I}_R \rho_{stat}\right] \ , \tag{S39}$$

where $\mathcal{I}_R = \mathcal{I}_R^+ - \mathcal{I}_R^-$ is the current superoperator. Naturally, $\mathcal{I}_L$ can be obtained analogously.

S2 Single-site molecular junction

Apart from studying the two-site systems, which are the main focus of this work, let us also consider a single-site molecule. It is described by a Hamiltonian analogous to (1) with

$$H_{\mathrm{M}} = \varepsilon_0\, a^\dagger a \ , \tag{S40}$$

which describes a single orbital that is coupled to both the source and drain electrodes and a phonon bath (via a Hamiltonian analogous to the one in the main body of this work).

In this simple system, it is possible to arrive at an analytical expression for the electric current (within the Born-Markov approximation with respect to the leads and the phonon bath). Due to the absence of intramolecular dynamics in this model system (and second order treatment of the molecule-lead interactions), the pure dephasing has no effect on the overall dynamics. Similarly, the Redfield approach now reduces to the pure dephasing approximation with the dephasing rate:

$$\gamma_{RD} = \int_0^\infty \mathrm{d}\tau \int_0^\infty \mathrm{d}\omega J(\omega)\left(\cos(\omega\tau)\coth(\beta\omega/2) \pm \mathrm{i}\sin(\omega\tau)\right) \ . \tag{S41}$$

Thus, within these two techniques the current through the system can be shown to be:

$$I = \frac{\Gamma_L\,\bar{\Gamma}_R - \Gamma_R\,\bar{\Gamma}_L}{\Gamma_L + \Gamma_R + \bar{\Gamma}_L + \bar{\Gamma}_R} \ , \tag{S42}$$

where $\Gamma_j = 2\pi\varrho_j|V_j|^2 f_j(\varepsilon_0)$, and $\bar{\Gamma}_j = 2\pi\varrho_j|V_j|^2[1 - f_j(\varepsilon_0)]$.

As mentioned before, unlike the Redfield and the pure dephasing approaches, the Polaron method also captures the vibrational effects at the molecule-lead interfaces. Within this technique the can still be expressed in the form Eq. (S42) but now with the hopping rates defined as:

$$\Gamma_j = \mathrm{Re}\, 2|V_j\varrho_j|^2 \int_{-\infty}^{\infty} \mathrm{d}\Omega\; f_j(\Omega + \varepsilon_0) \int_0^{\infty} \mathrm{d}\tau e^{i\Omega\tau} C^P(\tau)\;, \tag{S43}$$

$$\bar{\Gamma}_j = \mathrm{Re}\, 2|V_j\varrho_j|^2 \int_{-\infty}^{\infty} \mathrm{d}\Omega\; (1 - f_j(\Omega + \varepsilon_0)) \int_0^{\infty} \mathrm{d}\tau e^{i\Omega\tau} C^P(\tau)\;, \tag{S44}$$

where $C^P(\tau)$ is a correlation function as defined in Eq. (S25). Let us note here that in the limit of high bias (in both the Redfield and Polaron methods) it can be shown that $\Gamma_L = 2\pi|V_L|^2$, and $\bar{\Gamma}_R = 2\pi\varrho_j|V_R|^2$ (or vice-versa) so that all the approaches used here yield the same value of current $I = 2\pi\varrho_j|V_L|^2|V_R|^2/(|V_L|^2 + |V_R|^2)$.

The calculated IV characteristics (using the Polaron method) for the single-site system are shown in Fig. S1 assuming that the electronic degrees of freedom are coupled to a phonon bath with a superohmic SD:

$$\mathcal{J}(\omega) = \frac{\lambda}{2}\frac{\omega^3}{\omega_{\mathrm{c}}^3} e^{-\omega/\omega_{\mathrm{c}}}\;. \tag{S45}$$

Coupling of the electronic degrees of freedom to the phonon bath has several effects on the transport characteristics of the studied system. Firstly, it leads to a significant broadening of the IV curves (an effect we refer to as *phonon broadening*). As the bias increases, tunnelling into higher vibrational-electronic levels becomes possible. In the case of coupling to a single vibrational mode this results in equidistant steps in the current-voltage characteristics. Here, due to coupling to a phonon bath with a continuous SD, it results in broadened IV curves. Secondly, at high temperatures the system-bath coupling can lift the Coulomb blockade, as shown in Fig. S1. This can be explained as follows: electron-phonon interactions lead to fluctuations of the site energy. If the thermal energy is large enough, the magnitude of these fluctuations can be greater than the charging energy. The blockade can naturally also be lifted by broadening of the Fermi distributions in the leads. It is nonetheless interesting that the same effect can result purely

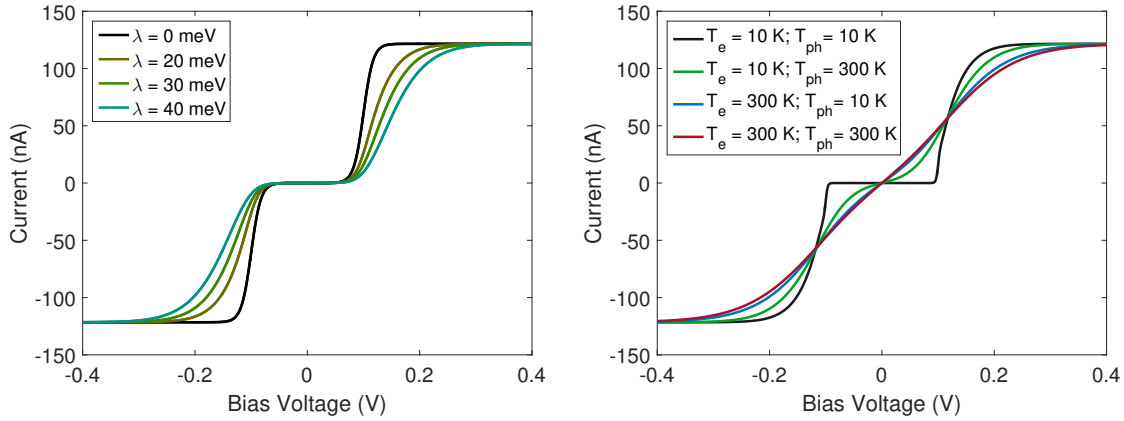

(a) (b)

Figure S1: IV characteristics of a single-site system coupled to a phonon bath obtained using the polaron treatment; $\varepsilon_0 = 50$ meV. (a) Calculated for different values of λ with $\omega_c = 5$ meV, and $T_e = T_{ph} = 50$ K. (b) Calculated for various temperatures with $\lambda = 20$ meV and $\omega_c = 5$ meV.

form phononic coupling. Finally, strong electron-phonon coupling can result in a suppression of current at low voltages: the effect known as the Franck-Condon blockade [12] (not shown).

S3 Two-site molecular junction

Let us now return to the two-site molecular system which is the main focus of this work. We begin by considering the values of the current in the absence of environmental interactions. The QME we have derived in Eq. (S7) gives for the current flowing through the system at low bias (i.e when only the LUMO level is found within the bias window):

$$I = e\,\frac{4J^2\gamma_L\gamma_R}{8J^2(\gamma_L+\gamma_R)+2\eta(\varepsilon_R-\varepsilon_L)(\gamma_L-\gamma_R)+\gamma_L\gamma_R^2+2(\gamma_L+\gamma_R)(\varepsilon_L-\varepsilon_R)^2}\,, \tag{S46}$$

for electrons flowing from left to right. Besides being limited to small bias, the above expression relies on the assumption of low temperature and weak molecule-lead couplings (for which treating H_V as a perturbation is justified). By contrast, for the case of high bias voltages, we recover the well-known result for the current flowing through a double quantum dot structure [13, 14]:

$$I = e\,\frac{4J^2\gamma_L\gamma_R}{4J^2\gamma_R^2+4\gamma_L\left((\varepsilon_R-\varepsilon_L)^2+2J^2\right)(\gamma_L-\gamma_R)+\gamma_L\gamma_R^2}\,. \tag{S47}$$

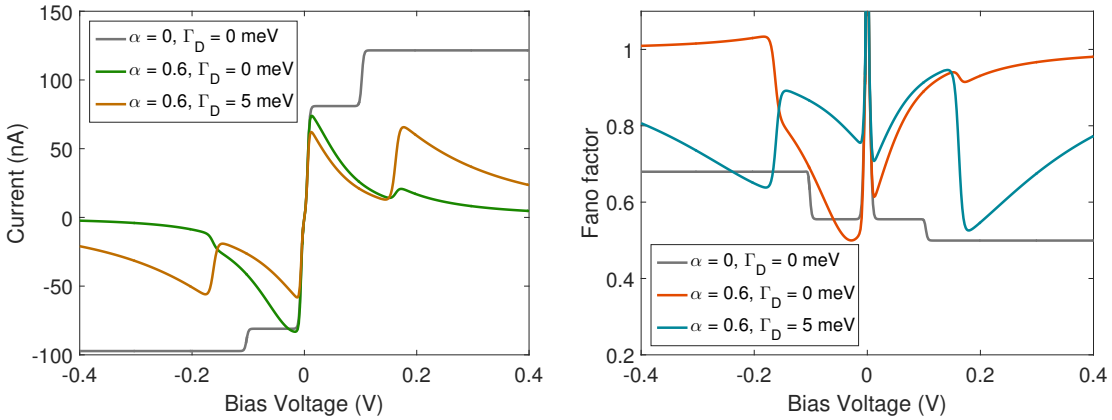

(a) IV characteristics (b) Fano factor

Figure S2: (a) IV characteristics and (b) Fano factor in the case of asymmetric coupling: $\gamma_R = 1$ meV, $\gamma_L = 2$ meV. Other parameters as in Fig. 2(a).

Here, we can also consider the case of asymmetric coupling of the molecule to the source and drain electrodes (we set $\gamma_L = 2\gamma_R$ but for simplicity assume that the capacitive coupling is still symmetric), see Fig. S2. Introducing asymmetric coupling results in asymmetric IV characteristics and bias dependence of Fano factor. Furthermore, one can now observe a super-Poissonian dynamics (F greater than 1) at intermediate bias voltage (*c.f* Kiesslich *et al.* [15]). Nonetheless, the main conclusions drawn from the symmetric case (in the main body of this work) remain unaffected by introducing the coupling asymmetry into the model.

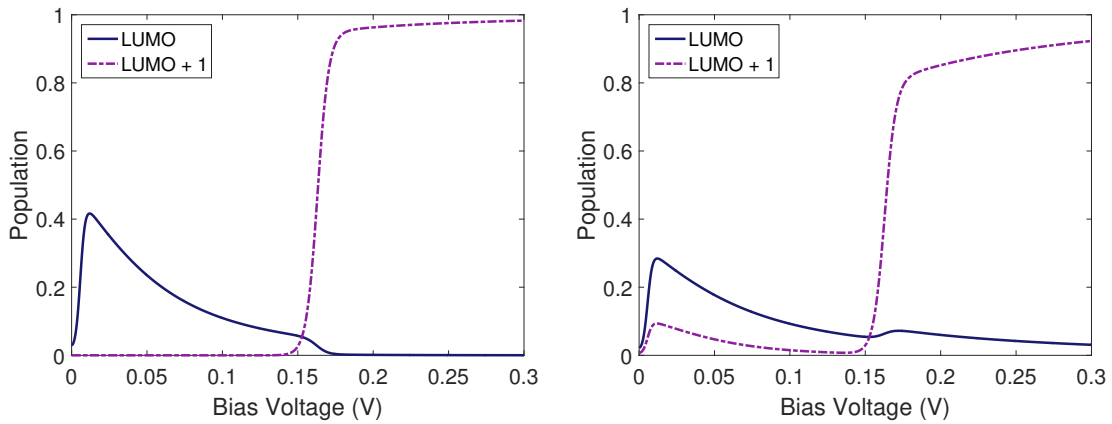

(a) $\Gamma_D = 0$ meV (b) $\Gamma_D = 1$ meV

Figure S3: Populations of LUMO and LUMO+1 levels in the (a) absence and (b) presence of pure dephasing. All parameters as in Fig. 2(a).

Let us now come back to a statement made in the main body of this work regarding the suppression of the transport through the LUMO level [Fig. 2(a)]. As we have stated this effect

stems from the dephasing-driven population transfer between LUMO and LUMO+1. Fig. S3 demonstrates that this is indeed the case: the LUMO+1 level is significantly populated at low bias in the presence of pure dephasing whilst remaining unoccupied for $\Gamma_D = 0$.

Finally let us also discuss the IV characteristics in the presence of dephasing but in the absence of capacitive coupling ($\alpha = 0$). Firstly, we can assume that the two sites are degenerate

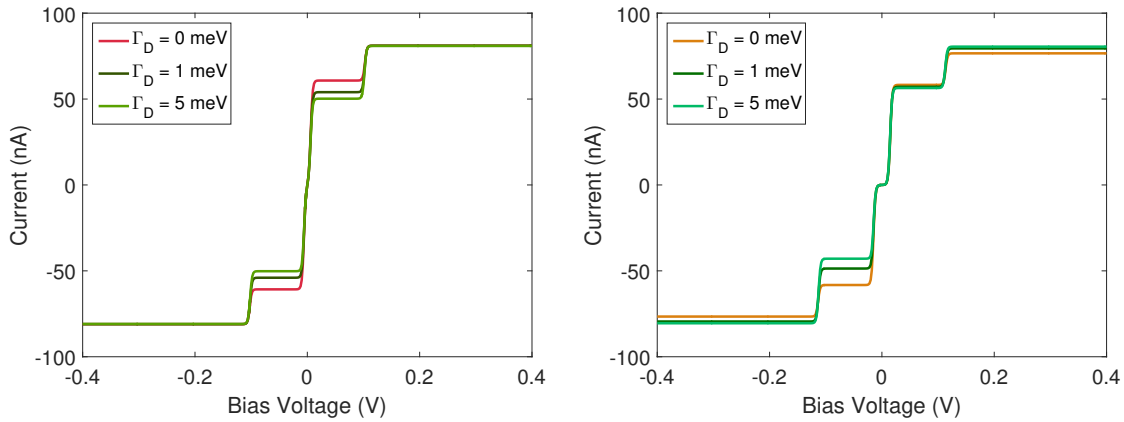

(a) $\varepsilon_L = \varepsilon_R = 27$ meV (b) $\varepsilon_L = 27$ meV; $\varepsilon_R = 37$ meV

Figure S4: IV characteristics in the absence of capactive coupling ($\alpha = 0$) but with pure dephasing present at the rate Γ_D. All parameters other in Fig. 2(a).

($\varepsilon_L = \varepsilon_R$), Fig. S4(a). Then, pure dephasing leads to a suppression of current at first plateau (which can once again be explained by the dephasing-induced population transfer), and a much less pronounced decrease in current at high bias voltage. There is no energy barrier for the left-to-right transition, and as a result dephasing only retards the otherwise efficient unitary evolution.

Alternatively, we can set a constant energy difference between the two site orbitals (note that this introduces asymmetry in the IV characteristics). Then, dephasing is going to increase the current flowing through the molecule at high bias, Fig. S4(b). At low bias (when only the LUMO orbital is found within the bias window), the effect will depend on the size of the energy gap: if this energy gap is small, the current will be reduced by dephasing due to the population transfer discussed in the manuscript, as shown in Fig. S4(a). If the energy gap is very large, dephasing can lead to an increase in the current by assisting the charge transfer transition across the energy gap.

S4 Limitations of the pure dephasing model

The central idea of the pure dephasing approach is to assume that the phononic dissipator in the QME is given by Eq. (S10). It corresponds to an exponential decay of inter-site coherences. As we have discussed, the pure dephasing approach effectively yields infinite-temperature behaviour (i.e. upward and downward transitions between the hybridised eigenstates occur with equal rates). This means that, for instance, in a simple Donor-Acceptor system in the steady-state limit the additional charge density will be equally likely found on the Donor and the Acceptor, irrespective of the energy difference between them.

This has several implications for our model: The upper bound on the current (in the presence of dephasing) is given by the value of current in the absence of environmental interactions, and for $\alpha = 0$ [grey line in Fig. 2(a)]. Such a bound does not hold – and can be violated (see Fig. 4) – when using more rigorous microscopically derived approaches.

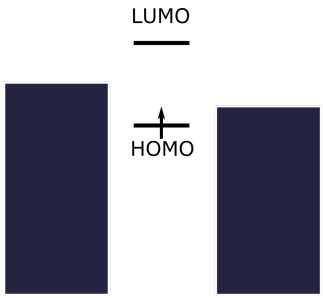

Figure S5: Schematic energy diagram for the system studied in Fig. S6(a).

It is also interesting to consider a case of a different energetic alignment of the molecular orbitals as compared to the one studied in the main body of this work. Let us set $\varepsilon_0 = 10$ meV. That means the one of the considered MOs is above and one is below the Fermi energy (and so in this Section we will refer to them as HOMO and LUMO levels, respectively), as schematically shown in Fig. S5.

The IV characteristics for this case are calculated in the absence and presence of pure dephasing, see Fig. S6(a). At low bias (and in the absence of dephasing), the HOMO level is fully occupied, the LUMO level is empty and since neither of them lies within the bias window there is no current flowing through the system. As we increase the bias we see the usual NDC behaviour (grey curve). Introducing dephasing phenomenologically [using Eq. (S10)] leads to a

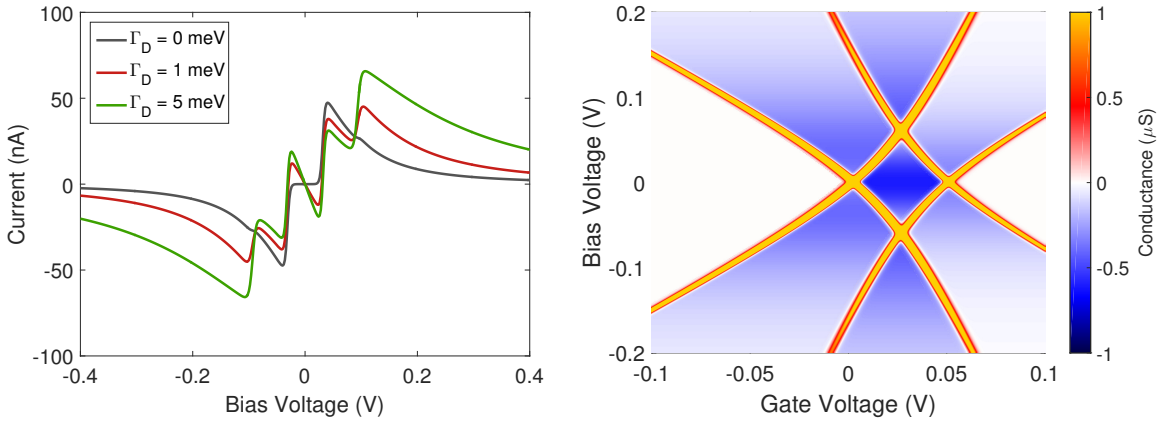

(a) (b)

Figure S6: (a) *IV* characteristics of a two-site system in the presence of dephasing at the rate Γ_{D}. (b) Conductance map with $\Gamma_{\mathrm{D}} = 1$ meV. In both figures $\varepsilon_0 = 10$ meV, $\alpha = 0.6$, and $T_{\mathrm{e}} = 10$ K.

surprising behaviour: electric current at low bias flows in the opposite direction to the applied bias! Pure dephasing results in population transfer from HOMO to LUMO, and since the LUMO level lies outside of the bias window, this charge density can tunnel out into both of the leads. Because of the energetic detuning present within our model, the LUMO level is predominantly centred on the left site, and so the charge density predominantly tunnels out into the source electrode – leading to negative current at positive bias and vice versa. This is clearly an example of a *qualitative* failure of the pure dephasing model[1].

We can, similarly to what has been done in the main body of this work, calculate a conductance map for our system, this time in the presence of pure dephasing – see Fig. S6(b). It clearly shows the effect described above. Interestingly, pure dephasing is also capable of lifting the Coulomb blockade for positive gate potentials [*c.f.* Fig. 2(b)].

[1]Such seemingly paradoxical behaviour can, in fact, also be obtained within the Redfield approach (for an ohmic SD) at high temperature. This requires, however, to artificially separate the phononic and electronic temperatures, and keep the latter close to zero.

S5 Marcus theory as the high-temperature limit of the Polaron method

In this Section, we demonstrate that the well-known Marcus theory [16] can be derived as a high temperature limit of our theoretical treatment. For simplicity, we consider a Donor–Acceptor (D–A) pair in which each of the sites is coupled to its own phonon bath. Within our formalism such a system is governed by the Hamiltonian:

$$H_{\mathrm{DA}} = \sum_{j=D,A} \bar{\varepsilon}_j a_j^\dagger a_j + \sum_{q_j} \omega_{q_j} b_{q_j}^\dagger b_{q_j} + g_{q_j} a_j^\dagger a_j (b_{q_j}^\dagger + b_{q_j}) + J(a_D^\dagger a_A + \mathrm{H.c.}) \ . \tag{S48}$$

Following the polaron transformation, we can redefine $\bar{H}_{\mathrm{DA}}$ as a sum of the system ($H_{\mathrm{S}}^{(\mathrm{DA})}$), environment ($H_{\mathrm{B}}^{(\mathrm{DA})}$), and interaction ($H_{\mathrm{I}}^{(\mathrm{DA})}$) Hamiltonian analogously to what has been done above:

$$\bar{H}_{\mathrm{S}}^{(\mathrm{DA})} = \sum_{j=\mathrm{D,A}} \bar{\varepsilon}_j a_j^\dagger a_j + J\langle B_{\mathrm{DA}}\rangle (a_D^\dagger a_A + \mathrm{H.c.}) \ ; \tag{S49}$$

$$H_{\mathrm{E}}^{(\mathrm{DA})} = \sum_{j=\mathrm{D,A}} \sum_{q_j} \omega_{q_j} b_{q_j}^\dagger b_{q_j} \ ; \tag{S50}$$

$$\bar{H}_{\mathrm{I}}^{(\mathrm{DA})} = J\left(\mathcal{B}\, a_D^\dagger a_A + \mathrm{H.c.}\right) \ . \tag{S51}$$

All the definitions follow from Section S1. In particular, $\mathcal{B} = B_D^\dagger B_A - \langle B_{\mathrm{DA}}\rangle$, and

$$\langle B_{\mathrm{DA}}\rangle = \prod_{j=\mathrm{D,A}} \exp\left(-\frac{1}{2}\int_0^\infty \mathrm{d}\omega \frac{\mathcal{J}_j(\omega)}{\omega^2} \coth\left(\frac{\omega}{2kT}\right)\right) \ . \tag{S52}$$

Here, in order to derive the Marcus theory we will work in the interaction picture of $H_{\mathrm{S2}}^{(\mathrm{DA})} = \sum_{j=\mathrm{D,A}} \bar{\varepsilon}_j a_j^\dagger a_j$. The time-evolution of the total density matrix ρ_{tot} is given by:

$$\frac{\mathrm{d}\tilde{\rho}_{tot}(t)}{\mathrm{d}t} = -\mathrm{i}[\tilde{H}_J^{(DA)}(t), \tilde{\rho}_{tot}(t)] - \int_0^t \mathrm{d}\tau \ \mathrm{Tr}_E\left[\tilde{H}_I(t), [\tilde{H}_J(\tau) + \tilde{H}_I(\tau), \tilde{\rho}_{tot}(\tau)]\right] \ , \tag{S53}$$

where $\tilde{A}(t)$ denotes operator A in an interaction picture of $H_{\rm S2}^{\rm (DA)}$ (as well as the polaron frame), and $H_J^{(DA)} = J\langle B_{\rm DA}\rangle(a_D^\dagger a_A + {\rm H.c.})$.

Within the Born-Markov and the secular approximations, the overall QME (in the polaron frame, and back in the Schrödinger picture) can be reduced to:

$$\frac{{\rm d}\bar{\rho}(t)}{{\rm d}t} = -{\rm i}[\bar{H}_S^{(DA)}, \bar{\rho}(t)] + \gamma_1\left(s^\dagger\bar{\rho}(t)s - ss^\dagger\bar{\rho}(t)\right) + \gamma_2\left(s\bar{\rho}(t)s^\dagger - \bar{\rho}(t)s^\dagger s\right) + \gamma_3\left(s\bar{\rho}(t)s^\dagger - s^\dagger s\bar{\rho}(t)\right) + \gamma_4\left(s^\dagger\bar{\rho}(t)s - \bar{\rho}(t)ss^\dagger\right) \ , \quad \text{(S54)}$$

where, for simplicity, $s = a_D^\dagger a_A$. Let us note here that in going from Eq. (S53) to Eq. (S54) the term linear in H_I vanished since ${\rm Tr}_E[H_I] = 0$. The rates in Eq. (S54) can be shown to be:

$$\gamma_1 = |J|^2\int_0^\infty {\rm d}\tau\ {\rm Tr_E}\left[\mathcal{B}\,\mathcal{B}^\dagger(-\tau)\rho_E\right]e^{-{\rm i}\Delta\varepsilon\tau} \ , \quad \text{(S55)}$$

$$\gamma_2 = |J|^2\int_0^\infty {\rm d}\tau\ {\rm Tr_E}\left[\mathcal{B}^\dagger(-\tau)\,\mathcal{B}\rho_E\right]e^{-{\rm i}\Delta\varepsilon\tau} \ , \quad \text{(S56)}$$

$$\gamma_3 = |J|^2\int_0^\infty {\rm d}\tau\ {\rm Tr_E}\left[\mathcal{B}^\dagger\,\mathcal{B}(-\tau)\rho_E\right]e^{{\rm i}\Delta\varepsilon\tau} \ , \quad \text{(S57)}$$

$$\gamma_4 = |J|^2\int_0^\infty {\rm d}\tau\ {\rm Tr_E}\left[\mathcal{B}(-\tau)\,\mathcal{B}^\dagger\rho_E\right]e^{{\rm i}\Delta\varepsilon\tau} \ , \quad \text{(S58)}$$

where we have defined $\Delta\varepsilon = \bar{\varepsilon}_D - \bar{\varepsilon}_A$.

We will now proceed to ignore the imaginary parts of γ_i (which result only in the renormalisation of the Hamiltonian) and notice that:

$${\rm Re}(\gamma_1) = {\rm Re}(\gamma_4) \equiv k_{\rm DA}/2 \ , \quad \text{(S59)}$$

$${\rm Re}(\gamma_2) = {\rm Re}(\gamma_3) \equiv k_{\rm AD}/2 \ , \quad \text{(S60)}$$

so that the QME (S54) can be written in the Lindblad form:

$$\frac{{\rm d}\bar{\rho}(t)}{{\rm d}t} = -{\rm i}[\bar{H}_S^{(DA)}, \bar{\rho}(t)] + k_{\rm DA}\left(s^\dagger\bar{\rho}(t)s - \frac{1}{2}ss^\dagger\bar{\rho}(t) - \frac{1}{2}\bar{\rho}(t)ss^\dagger\right) + k_{\rm AD}\left(s\bar{\rho}(t)s^\dagger - \frac{1}{2}\bar{\rho}(t)s^\dagger s - \frac{1}{2}s^\dagger s\bar{\rho}(t)\right) \ . \quad \text{(S61)}$$

In the above k_{DA} (k_{AD}) corresponds to the rate of hopping from D to A (and vice-versa).

Moving into the high temperature limit, we take $\coth(\omega/2kT) \approx 2kT/\omega$, and we will also assume a slowly fluctuating environment so that $\sin(\omega\tau) \approx \omega\tau$ and $\cos(\omega\tau) \approx 1-\omega^2\tau^2/2$. Then,

$$\frac{k_{\mathrm{DA}}}{2|J|^2} = \mathrm{Re}\int_0^\infty \mathrm{d}\tau \exp\left[-kT\lambda\,\tau^2\right] \exp\left[-\mathrm{i}(\lambda-\Delta\varepsilon)\tau\right] \ , \tag{S62}$$

and equivalently for k_{AD}. Here, λ is the overall reorganisation energy, which is the sum of reorganisation energies of the donor and acceptor sites $\lambda = \lambda_{\mathrm{D}} + \lambda_{\mathrm{A}}$, where

$$\lambda_j = \int_0^\infty \mathrm{d}\omega \frac{\mathcal{J}_j(\omega)}{\omega} \ . \tag{S63}$$

Finally, we obtain:

$$k_{\mathrm{DA}} = |J|^2\sqrt{\frac{\pi}{\lambda kT}}\exp\left(-\frac{(\lambda-\Delta\varepsilon)^2}{4\lambda kT}\right) \ , \tag{S64}$$

$$k_{\mathrm{AD}} = |J|^2\sqrt{\frac{\pi}{\lambda kT}}\exp\left(-\frac{(\lambda+\Delta\varepsilon)^2}{4\lambda kT}\right) \ . \tag{S65}$$

Furthermore, for ohmic spectral densities $\mathcal{J}_j$ the polaron renormalisations in Eq. (S49) are equal to zero, so that

$$H_{\mathrm{S}}^{(\mathrm{DA})} = \sum_{j=\mathrm{D,A}} \bar{\varepsilon}_j a_j^\dagger a_j \ . \tag{S66}$$

Let us note here that the above equality does not hold in the case of superohmic SDs. However, in that case the polaron renormalisation terms [Eq. (S52)] vanish in the limit of high temperature so that the unitary component of the D–A transition can again be ignored.

In summary, we have shown that in the limit of high temperature (and for a slowly fluctuating environment) the polaron treatment reduces to Marcus theory with electron hopping rates given by Eq. (S64, S65).

References

[1] M. L. Perrin, R. Frisenda, M. Koole, J. S. Seldenthuis, J. A. C. Gil, H. Valkenier, J. C. Hummelen, Ni. Renaud, Fer. C. Grozema, J. M. Thijssen, et al. Large negative differential conductance in single-molecule break junctions. *Nat. Nanotechnol.*, 9(10):830–834, 2014.

[2] H. Valkenier, C. M. Guédon, T. Markussen, K. S. Thygesen, S. J. van der Molen, and J. C. Hummelen. Cross-conjugation and quantum interference: a general correlation? *Phys. Chem. Chem. Phys.*, 16(2):653–662, 2014.

[3] M. L. Perrin, E. Galán, R. Eelkema, J. M. Thijssen, F. Grozema, and H. S. J. van der Zant. A gate-tunable single-molecule diode. *Nanoscale*, 8(16):8919–8923, 2016.

[4] H.-P. Breuer and F. Petruccione. *The Theory of Open Quantum Systems*. Oxford University Press on Demand, 2002.

[5] P. Zedler, G. Schaller, G. Kiesslich, C. Emary, and T. Brandes. Weak-coupling approximations in non-markovian transport. *Phys. Rev. B*, 80(4):045309, 2009.

[6] C. Flindt, T. Novotnỳ, A. Braggio, M. Sassetti, and A.-P. Jauho. Counting statistics of non-markovian quantum stochastic processes. *Phys. Rev. Lett.*, 100(15):150601, 2008.

[7] A. Nazir and D. P. S. McCutcheon. Modelling exciton–phonon interactions in optically driven quantum dots. *J. Phys.: Condens. Matter*, 28(10):103002, 2016.

[8] I. G. Lang and Y. A. Firsov. Kinetic theory of semiconductors with low mobility. *Sov. Phys. JETP*, 16(5):1301, 1963.

[9] C. Flindt, T. Novotnỳ, and A.-P. Jauho. Full counting statistics of nano-electromechanical systems. *EPL*, 69(3):475, 2005.

[10] C. Flindt, T. Novotnỳ, and A.-P. Jauho. Current noise in a vibrating quantum dot array. *Phys. Rev. B*, 70(20):205334, 2004.

[11] C. Schinabeck, R. Härtle, H. B. Weber, and M. Thoss. Current noise in single-molecule junctions induced by electronic-vibrational coupling. *Phys. Rev. B*, 90(7):075409, 2014.

[12] J. Koch and F. von Oppen. Franck-condon blockade and giant fano factors in transport through single molecules. *Phys. Rev. Lett.*, 94(20):206804, 2005.

[13] S. A. Gurvitz and Y. S. Prager. Microscopic derivation of rate equations for quantum transport. *Phys. Rev. B*, 53(23):15932, 1996.

[14] T. H. Stoof and Y. V. Nazarov. Time-dependent resonant tunneling via two discrete states. *Phys. Rev. B*, 53(3):1050, 1996.

[15] G. Kießlich, E. Schöll, T. Brandes, F. Hohls, and R. J. Haug. Noise enhancement due to quantum coherence in coupled quantum dots. *Phys. Rev. Lett.*, 99(20):206602, 2007.

[16] R. A. Marcus. Electron transfer reactions in chemistry: theory and experiment (nobel lecture). *Angew. Chem. Int. Ed.*, 32(8):1111–1121, 1993.